Journal of Mammary Gland Biology and Neoplasia (2025) 30:1
https://doi.org/10.1007/s10911-025-09574-8

RESEARCH

Defective Mammary Epithelial Outgrowth in Transgenic EKAREV–NLS Mice: Correction via Estrogen Supplementation and Genetic Background Modification

Matea Brezak[1] · **Zuzana Sumbalova Koledova**[1,2]

Received: 12 September 2024 / Accepted: 8 January 2025

Abstract
Fluorescent biosensors offer a powerful tool for tracking and quantifying protein activity in living systems with high temporospatial resolution. However, the expression of genetically encoded fluorescent proteins can interfere with endogenous signaling pathways, potentially leading to developmental and physiological abnormalities. The EKAREV-NLS mouse model, which carries a FRET-based biosensor for monitoring extracellular signal-regulated kinase (ERK) activity, has been widely utilized both in vivo and in vitro across various cell types and organs. In this study, we report a significant defect in mammary epithelial development in EKAREV-NLS C57BL/6J female mice. Our findings reveal that these mice exhibit severely impaired mammary epithelial outgrowth, linked to systemic defects including disrupted estrous cycling, impaired ovarian follicle maturation, anovulation, and reduced reproductive fitness. Notably, estrogen supplementation was sufficient to enhance mammary epithelial growth in the EKAREV-NLS C57BL/6J females. Furthermore, outcrossing to the ICR genetic background fully restored normal mammary epithelial outgrowth, indicating that the observed phenotype is dependent on genetic background. We also confirmed the functional performance of the biosensor in hormone-supplemented and outcrossed tissues through time-lapse imaging of primary mammary epithelial cells. Our results underscore the critical need for thorough characterization of biosensor-carrying models before their application in specific research contexts. Additionally, this work highlights the influence of hormonal and genetic factors on mammary gland development and emphasizes the importance of careful consideration when selecting biosensor strains for mammary studies.

Keywords EKAREV–NLS mouse · Estradiol supplementation · ERK signaling · Biosensor · Mammary epithelium · Genetic background · Hormonal imbalance

Introduction

Fluorescent biosensors are powerful tools in biological research, which employ fluorescent molecules to report on the presence or activity of specific biological targets, and thus detect and measure various cellular processes in real-time. Among the most advanced types of fluorescent biosensors are FRET (Förster resonance energy transfer) biosensors. FRET biosensors operate on the principle that energy can be transferred non-radiatively from a donor fluorophore to an acceptor fluorophore when they are in close proximity, typically less than 10 nanometers. The efficiency of this energy transfer depends on the distance between the two fluorophores, making FRET biosensors ideal for monitoring dynamic interactions, such as protein-protein interactions, conformational changes within molecules, or catalytic functions.

Biosensors can be used in vitro as well as in vivo, where they can be expressed constitutively in all cells or conditionally upon induction, e.g. in a specific cell type. However, the expression of biosensors in mice, particularly those involving genetically encoded reporters or fluorescent proteins, can have potentially negative effects on mouse viability, reproductive fitness, or other physiological processes.

✉ Zuzana Sumbalova Koledova
zuzana.sumbalova-koledova@img.cas.cz

[1] Department of Histology and Embryology, Faculty of Medicine, Masaryk University, Brno, Czech Republic

[2] Institute of Molecular Genetics of the Czech Academy of Sciences, Prague, Czech Republic

Published online: 18 January 2025

Potential negative effects depend on factors like the type of biosensor, its expression level, and the genomic location of its insertion.

Cells expressing foreign genes (e.g. for fluorescent proteins) are not always healthy and viable, particularly when used in vivo [1] and the reporter protein is present in high concentrations or produces a cytotoxic metabolite [2]. Green fluorescent protein (GFP) and its analogs show different levels of cellular toxicity [3, 4], mediated by reactive oxygen species production [5]. For instance, GFP expression increases oxidative stress and influences cell survival under stress conditions in neuroblastoma cell lines [6], and activates endoplasmic reticulum stress in breast cancer cells [7]. Yellow fluorescent protein (YFP) acts as an activator of a robust cell stress response in mouse neurons [8]. Moreover, the expression of foreign proteins can sometimes trigger immune responses [9]. Further, due to the lack of signal amplification possibility, biosensor expression must be relatively high. Strong promoters like CAG are often used for biosensor expression as they offer stable ubiquitous strong expression in all tissues. Some biosensors, particularly those based on fluorescent proteins like GFP, can be toxic when overexpressed [4]. Moreover, localization of the transgenic construct within the genome can influence cellular behavior or reproductive fitness. Random insertion of biosensor genes can disrupt endogenous genes or regulatory elements, leading to developmental abnormalities or lethality. Finally, a combination of the aforementioned effects of biosensor expression might be organ-specific. One study reported dose-dependent heart condition developed in mice overexpressing GFP [10]. The expression of genetically encoded calcium indicators in neurons can cause neurotoxicity [11], leading to behavioral abnormalities or reduced cognitive function.

EKAREV–NLS (Eisuke) mice carry a FRET-based biosensor of ERK1/2 phosphorylation activity [12]. The biosensor was first developed by Harvey et al. [13] and subsequently modified by Komatsu et al. [14]. It consists of two main functional domains and a linker chain. The sensory region contains a consensus MAPK target sequence (PRTP), WW phospho-binding domain, and ERK-specific (FQFP) docking site, while the reporter region includes a fluorescent protein FRET pair; CFP, and YFP. The transgenic mouse line was developed by Tol2-mediated gene transfer, through oocyte co-injection of the pT2A-EKAREV-NLS plasmid with Tol2 mRNA, producing the strain with several transgene integration sites and stable Mendelian transgene transmission [12]. The strain was successfully used for ERK dynamics investigations in the intestine [15, 16], skin [17, 18], and mammary tumor tissue [19] with no reported physiological abnormalities. We aimed to use the EKAREV-NLS mice to study the role of ERK signaling in mammary epithelial morphogenesis. Because the reports on its use in mammary tissue have been scarce, we assessed its suitability for studying ERK in mammary gland development. Here we report severe mammary epithelial phenotype in EKAREV-NLS mice, which is associated with the systemic effect of hormonal dysregulation, and reveal simple strategies to alleviate it.

Results

EKAREV–NLS Biosensor Influences Mammary Gland Morphology and Reproductive Fitness

Given the absence of prior reports on the use of the EKAREV-NLS (hereafter referred to as "EKAREV") strain in mammary gland research, we aimed to characterize and assess its suitability for studying ERK activity dynamics in mammary epithelial morphogenesis. To this end, we investigated mammary gland morphology in EKAREV positive (EKAREV+, hemizygous) and EKAREV negative (EKAREV−, wild-type) nulliparous female mice. At 10 weeks of age, all analyzed EKAREV+ mice showed significant alterations in epithelial morphology, characterized by markedly reduced epithelial outgrowth and a simplified branching pattern (Fig. 1a–c). Further examination of the mammary glands at later time points (10 to 19 weeks of age) revealed conservation of the impeded epithelial outgrowth and branching phenotype in the EKAREV+ mice, with occasionally increased fat pad penetration (Supplementary Fig. 1). Moreover, EKAREV+ females were smaller and had significantly lower body weight than the EKAREV− females (Fig. 1d, e), low visceral adipose tissue deposits and poor coat quality, which together with the mammary phenotype suggested a systemic effect.

Because the phenotype of EKAREV+ mammary glands resembled the mammary gland of mice ovariectomized before puberty [20], we suspected that it could be caused by dysregulation of female sex hormones. Therefore, we measured estrogen and progesterone levels in blood serum and examined ovaries and estrous cycle in the EKAREV mice. Interestingly, the level of freely circulating estrogen was significantly higher in EKAREV+ animals compared to the EKAREV− control, and a similar trend was apparent in progesterone levels (Fig. 1f, g). The ovaries of the majority (approx. 90%) of EKAREV+ mice were significantly smaller, with a reduced number of late-stage follicles and mostly undetectable corpora lutea, indicating disrupted estrous cycles and impaired ovulation (Fig. 1h, i; Supplementary Fig. 2). Moreover, when bred with wild-type males, EKAREV+ females frequently failed to produce offspring (Supplementary Fig. 3b). When EKAREV+ mothers

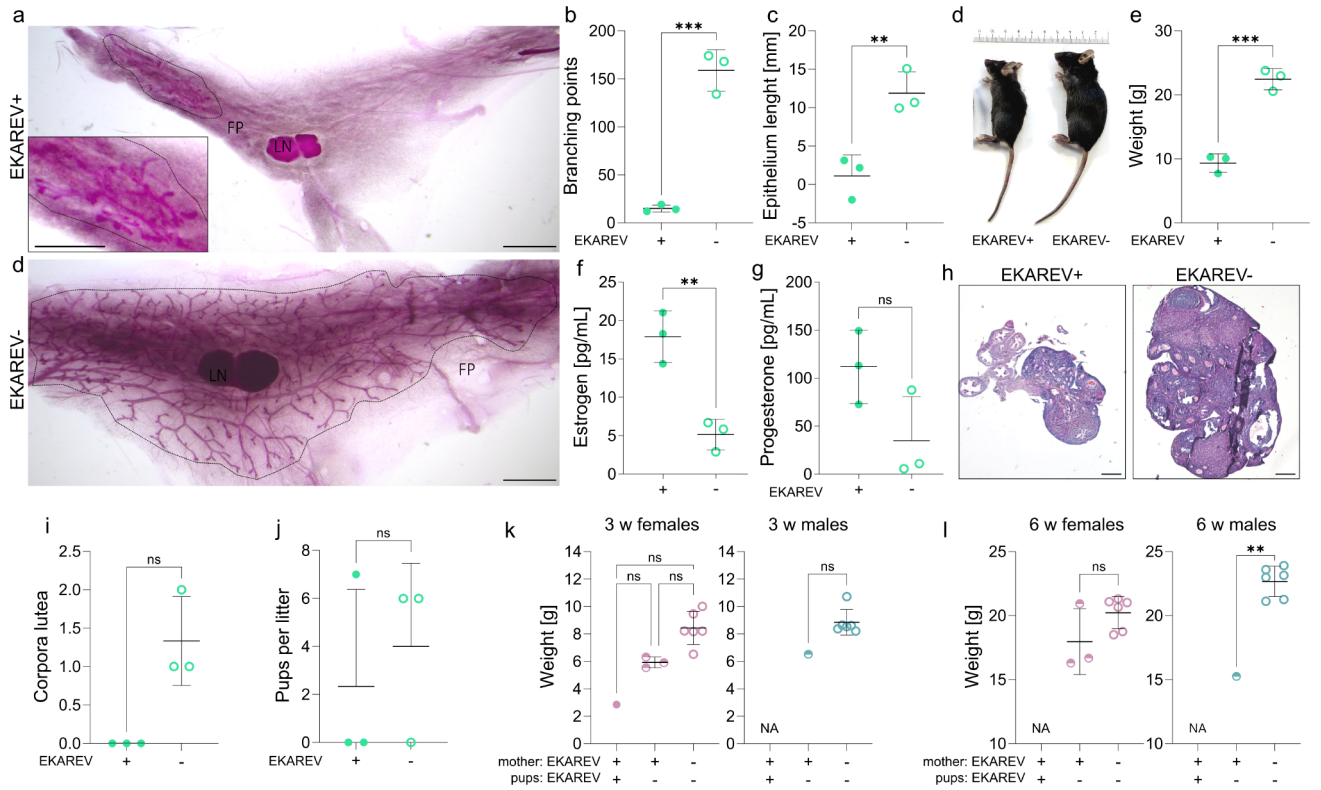

Fig. 1 EKAREV+ female mice exhibit retarded mammary epithelial outgrowth, lower body weight, and reduced reproductive fitness. (**a**) Carmine-stained mammary glands of EKAREV+ and EKAREV− 10-week-old mice. The white dashed line outlines the epithelial ductal tree area while the insert shows part of the EKAREV+ epithelial tree structure; FP, fat pad; LN, lymph node. Scale bar: 1 mm. (**b** and **c**) Quantification of mammary epithelial morphological descriptors. The plots show the number of branching points (sum of primary and secondary) (**b**) and the length of epithelial outgrowth from the center of the lymph node to the distal part of the gland (**c**) as mean ± SD; $N = 3$ EKAREV+, 3 EKAREV−; $^{**}p \leq 0.01$, $^{***}p \leq 0.001$ (Student's t-test). (**d**) Macroscopic comparison of 10-week-old nulliparous EKAREV+ (left) and EKAREV− (right) female mice. Scale bar: 1 cm. (**e**) Post-mortem whole-body weights of EKAREV+ and EKAREV− female mice. The plot shows mean ± SD; $N = 3$ EKAREV+, 3 EKAREV−; $^{***}p \leq 0.001$ (Student's t-test). (**f**) Hematoxylin- and eosin-stained sections from ovaries of EKAREV+ and EKAREV− 10-weeks-old females. Scale bar: 100 µm. (**g**) Quantification of the number of corpora lutea, counted in serial sections of ovaries (taken every 25 µm within the first half of the ovary). The plot shows mean ± SD; $N = 3$ EKAREV+, 3 EKAREV−; ns $p > 0.05$ (Student's t-test). (**h**, **i**) Level of reproductive hormones (**h**) estrogen, and (**i**) progesterone in circulating blood serum. The plots show mean ± SD. $N = 3$ EKAREV+, 3 EKAREV−; ns $p > 0.05$, $^{***}p \leq 0.001$ (Student's t-test). (**j**) The plot shows the total number of pups born from the breeding of EKAREV+ or EKAREV− females with wild-type ICR male as mean ± SD; $n = 3$ litters from EKAREV+ mother, 3 litters from EKAREV− mother; ns $p > 0.05$ (Student's t-test). (**k**, **l**) Weight of offspring from panel (**j**). The plots show body weight of 3-week-old (**k**) and 6-week-old (**l**) female (pink) and male (blue) pups as mean ± SD; $N = 17$ born pups of 3 EKAREV+ and 3 EKAREV− mothers; ns $p \geq 0.05$, $^{**}p \leq 0.01$ (Kruskal-Wallis test for 3 w females, Mann-Whitney test for 6 w females, Student's t-test for both 3 w and 6 w males)

produced offspring, the litters were smaller, with reduced viability and lower body weight despite normal maternal behavior of EKAREV+ mice (Fig. 1j). EKAREV+ offspring showed the lowest body weight (Fig. 1k, l), incomplete fur development, and poor viability. Further, EKAREV+ mothers showed delayed involution following the weaning of the pups at 3 weeks of age (Supplementary Fig. 3d). Collectively, this data suggests a profound disruption of female sex hormone signaling, which negatively impacts mammary gland development, follicular maturation, and reproductive capability.

Estradiol Supplementation Results in Partial Mammary Gland Phenotype Rescue

Given the well-established roles of estrogen and progesterone in mammary gland development and female reproductive system regulation [20–22], we hypothesized that supplementing these hormones might stimulate reproductive system function and mammary epithelial morphogenesis in EKAREV+ mice. We implemented a hormonal supplementation regimen via drinking water, as described in a previous study [23], with non-treated, estradiol-only, and combined estradiol-progesterone groups. Analysis of mammary gland morphology revealed a significant increase in

epithelial penetration and branching index in both estradiol-only and estradiol-progesterone treated groups compared to non-treated EKAREV+ mice, indicating a positive impact of the hormonal treatment on epithelial tree development and mammary gland morphology (Fig. 2a–c). Moreover, although epithelial branching and penetration improved in both treatment groups, the mammary branching complexity of the hormone-treated EKAREV+ mice did not reach the branching complexity of the EKAREV− mammary glands (Fig. 2a,b), suggesting only a partial rescue of the phenotype. The dual supplementation group showed an increased number of terminal end buds (TEB) at the time of sample collection, suggesting a greater growth potential in this group (Fig. 2d). Hormonal treatment of EKAREV− control animals had no significant impact on mammary gland morphology, suggesting a preserved signaling regulation in these animals (Supplementary Fig. 4).

To investigate the underlying mechanism of EKAREV+ phenotype and its rescue by hormonal supplementation, we investigated estrogen receptor (ER) expression in mammary epithelium by immunohistochemistry. Interestingly, we found no significant differences in ER expression levels between EKAREV+ non-treated animals, EKAREV+ hormone-treated and EKAREV− non-treated (control) animals (Fig. 2e, f). In pubertal and adult mice, estradiol signaling upregulates progesterone receptor (PR) expression, whose signaling exerts proliferative effects on mammary epithelium [24]. To determine whether this signaling axis was affected, we assessed PR and Ki67 expression. Importantly, we found significantly decreased expression of PR in EKAREV+ non-treated animals (Fig. 2e, g). Hormonal supplementation increased PR levels in both treatment groups (Fig. 2e, g) to levels comparable to the EKAREV− mice and thus partially restoring the signaling regulation necessary for normal epithelial development. Similarly, an increased proportion of proliferative (Ki67+) cells was detected in both treatment groups compared to EKAREV+ non-treated animals (Fig. 2e, h), indicating a restored PR signaling network in mammary epithelium.

Estradiol and progesterone, alongside gonadotropins, play crucial roles in ovarian follicle development, maturation, and ovulation [25]. We hypothesized that hormonal supplementation might enhance follicle content, which would further confirm the restoration of the regulatory axis. As expected, hormonal supplementation increased ovary size and the number of late-stage follicles (Fig. 2i, j; Supplementary Fig. 5) in both groups. However, unlike the dual estradiol-progesterone group, estradiol-only supplementation did not result in detectable corpus luteum formation in EKAREV+ mice, suggesting that a more robust stimulus is required to induce successful follicle maturation and/or ovulatory signals. Hormonally supplemented mice exhibited normal behavior and showed a trend of increased body weight (Fig. 2k). Furthermore, increased visceral fat deposits as well as improved coat quality were observed in both treatment groups. The end-point estrous cycle staging showed improved stage distribution more similar to the EKAREV− mice (Fig. 2l).

Fig. 2 Hormonal supplementation rescues the mammary gland phenotype of the EKAREV+ females. (**a**) Carmine-stained mammary glands of 14-week-old female mice after 5 weeks of hormonal supplementation. Scale bar: 1 mm. The inserts show details of the distal ends of the epithelial ductal tree. Scale bar: 500 µm. (**b**, **c**) Quantification of mammary epithelial morphological descriptors. The plots show the number of branching points (sum of primary and secondary) (**b**) and the length of epithelial outgrowth from the center of the lymph node to the distal part of the gland (**c**) as mean ± SD. $N = 10$ EKAREV+ NT, 10 EKAREV+ E2, 11 EKAREV+ E2P4, 17 EKAREV− NT; * $p \leq 0.05$, **** $p \leq 0.0001$ (Kruskal-Wallis test in (**b**) one-way ANOVA in (**c**). (**d**) The plot shows the number of TEBs as mean ± SD. $N = 10$ EKAREV+ E2, 11 EKAREV+ E2P4; ** $p \leq 0.01$ (Mann-Whitney test). (**e**) Estrogen receptor (ER), progesterone receptor (PR), and Ki67 expression in mammary gland epithelium of 14-week-old female mice after 5 weeks of hormonal supplementation. The inserts show details of epithelial areas. Scale bar: 100 µm. (**f**) Quantification of ER+ cell proportion in mammary epithelium. The plots show mean ± SD. $N = 17$ EKAREV+ NT, 21 EKAREV+ E2, 28 EKAREV+ E2P4, 13 EKAREV− NT; ns $p > 0.05$ (Student's t-test). (**g**) Quantification of PR+ cell proportion in mammary epithelium. The plots show mean ± SD. $N = 9$ EKAREV+ NT, 8 EKAREV+ E2, 9 EKAREV+ E2P4, 10 EKAREV− NT; *** $p \leq 0.001$ (one-way ANOVA). (**h**) Quantification of Ki67+ cell proportion in mammary epithelium. The plots show mean ± SD. $N = 10$ EKAREV+ NT, 9 EKAREV+ E2, 22 EKAREV+ E2P4, 12 EKAREV− NT; *** $p \leq 0.001$ (Student's t-test). (**i**) Hematoxylin- and eosin-stained sections of ovaries from 14-week-old females after 5 weeks of hormonal supplementation. Scale bar: 100 µm. (**j**) Quantification of a number of corpora lutea, counted in serial sections of ovaries (taken every 25 µm within the first half of the ovary). The plot shows mean ± SD. $N = 8$ EKAREV+ NT, 7 EKAREV+ E2, 11 EKAREV+ E2P4, 9 EKAREV− NT; ** $p \leq 0.01$, *** $p \leq 0.001$ (Kruskal-Wallis test). (**k**) The plot shows whole-body weights of hormone-supplemented females as mean ± SD. $N = 10$ EKAREV+ NT, 10 EKAREV+ E2, 11 EKAREV+ E2P4, 17 EKAREV− NT; * $p \leq 0.05$, ** $p \leq 0.01$, *** $p \leq 0.001$, **** $p \leq 0.0001$ (Kruskal-Wallis test). (**l**) Estrous cycle stage distribution in the cohort of hormone-supplemented females at the time of mammary and ovarian tissue collection. NT, non-treated; E2, 17β–estradiol-treated; E2P4, 17β–estradiol- and progesterone-treated; TEB, terminal end bud; PR, progesterone receptor

Change of Genetic Background Alleviates Biosensor Effect on Mammary Gland Morphology and Reproductive Fitness

Given that our 5-week hormonal supplementation experiments did not yield mammary epithelial three with full branching and fat pad penetration and have therefore only partially rescued the mammary gland phenotype, we sought to explore an alternative approach. Noting the reported significant effect of genetic background on mammary gland development and tumorigenesis [26, 27], we questioned whether the observed phenotype was genetic

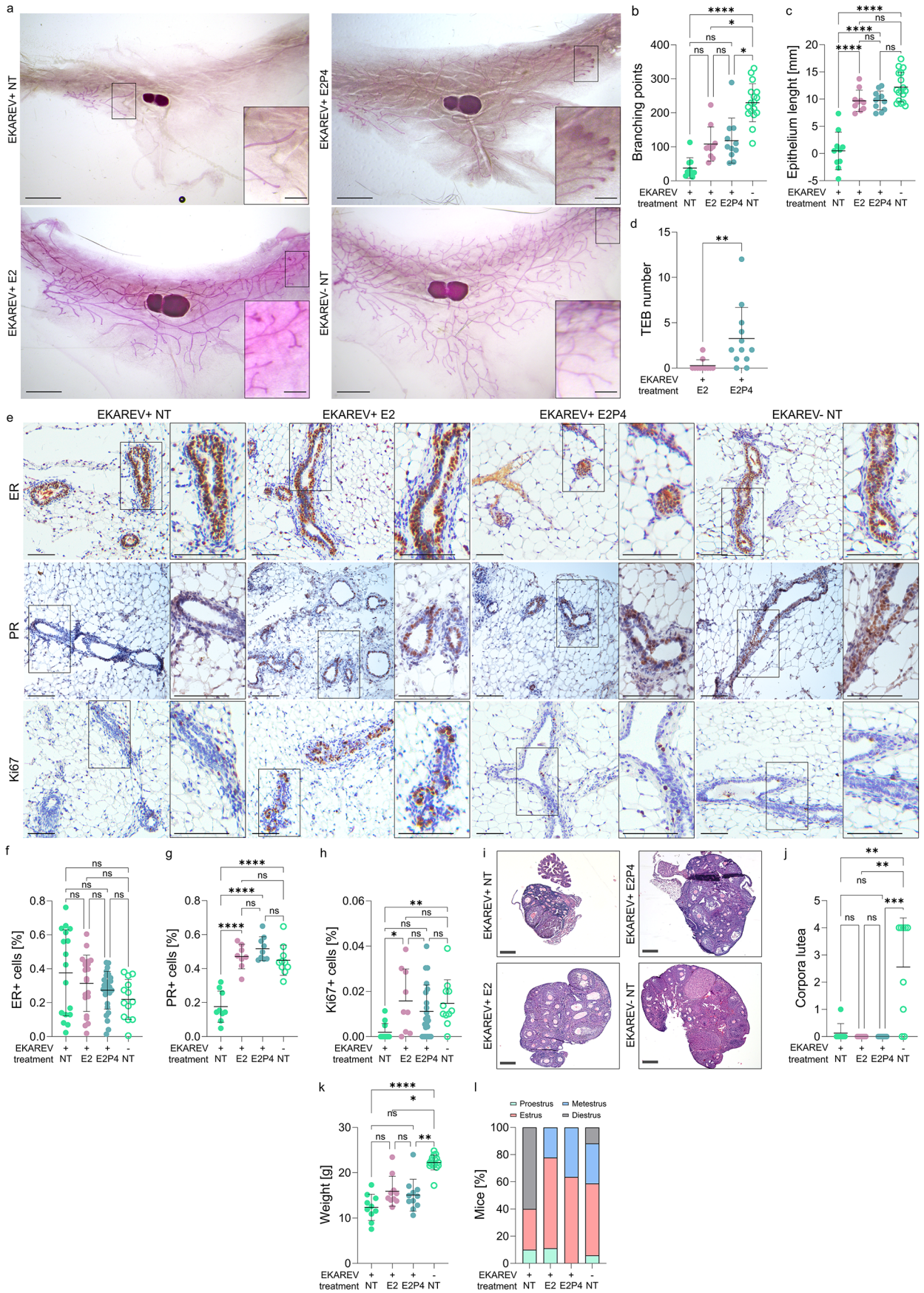
a
EKAREV+ NT
EKAREV+ E2P4
EKAREV+ E2
EKAREV- NT
b
Branching points
EKAREV treatment + NT + E2 + E2P4 - NT
c
Epithelium lenght [mm]
EKAREV treatment + NT + E2 + E2P4 - NT
d
TEB number
EKAREV treatment + E2 + E2P4
e
EKAREV+ NT
EKAREV+ E2
EKAREV+ E2P4
EKAREV- NT
ER
PR
Ki67
f
ER+ cells [%]
g
PR+ cells [%]
h
Ki67+ cells [%]
i
EKAREV+ NT
EKAREV+ E2P4
EKAREV+ E2
EKAREV- NT
j
Corpora lutea
k
Weight [g]
l
Proestrus
Metestrus
Estrus
Diestrus
Mice [%]

background dependent. To investigate this, we outcrossed EKAREV+C57BL/6J mice with wild-type ICR mice (Fig. 3a), an outbred strain known for its robust reproductive performance and rapid growth [28]. We then analyzed overall fitness, mammary gland morphology, ovarian follicle content, and reproductive performance. All analyzed outcrossed C57BL/6J×ICR 14-week-old EKAREV+ offspring showed no signs of compromised well-being, as they maintained good fur quality and showed no reduction in visceral body fat. However, they did have somewhat lower body weights compared to their EKAREV− littermates (Fig. 3b, c). The end-point estrous staging revealed similarities in the stage proportions between the groups (Fig. 3d).

Strikingly, we observed no differences in the appearance of the epithelial ductal tree in the outcrossed EKAREV+ and EKAREV− mice (Fig. 3e). Both groups displayed fully developed epithelial structures with well-formed primary and secondary branches extending into the distal mammary fat pad (Fig. 3f, g). Moreover, both EKAREV+ and EKAREV− outcrossed mice exhibited similar ER, PR, and Ki67 expression patterns, with a high percentage of receptor expressing and proliferative cells in the mammary epithelial compartment (Fig. 3h, k) and similar estrogen and progesterone levels (Fig. 3l-m). Aside from a slight reduction in ovary size in EKAREV+ outcrossed females, no significant differences in follicle counts were observed (Fig. 3n; Supplementary Fig. 6). Both EKAREV+ and EKAREV− outcrossed mice showed evidence of proper hormonal cycling and ovulation, as indicated by the presence of corpora lutea and a substantial number of late-stage follicles (Fig. 3o). When EKAREV+ and EKAREV− outcrossed mice were bred with ICR males, no significant differences were found in litter sex ratio or viability, but the EKAREV+ females produced fewer pups (Fig. 3p-r; Supplementary Fig. 7b, c). Pups from EKAREV+ mothers exhibited, in general, lower body weights than pups from EKAREV− mothers, and in particular EKAREV+ pups were lighter than their EKAREV− littermates. Nevertheless, none of the pups showed the developmental issues observed in EKAREV+ pups from C57BL/6J mothers. Both EKAREV+ and EKAREV− mothers showed normally involuting glands following the weaning of the pups (Supplementary Fig. 7d). These data suggest that the change of genetic background fully rescues mammary phenotype and restores reproductive system functionality in EKAREV+ mice.

Biosensor Function is Maintained Following Hormone Treatment and Background Change

Our results suggest that to use the EKAREV-NLS biosensor to study ERK signaling dynamics in mammary epithelial tissue, the EKAREV+C57BL/6J mice need to be supplemented by female sex hormones or outcrossed to a mixed C57BL/6J×ICR background to develop a properly branched mammary epithelial ductal structure. To determine whether hormonal supplementation or change of genetic background influence biosensor function in the target tissue, we set out to compare ERK activity patterns in primary mammary epithelial cells (MECs) isolated from non-treated, hormone-supplemented, and outcrossed mice.

First, we assessed overall EKAREV-NLS biosensor expression in primary MECs cultured in 2D. We observed

Fig. 3 Change of genetic background rescues the mammary gland phenotype of EKAREV+ females. (**a**) Schematic representation of outcross experiment and subsequent breeding experiment to assess reproductive fitness. Outcross was achieved by mating male EKAREV+C57BL/6J with wild-type ICR female. Female offspring was then used in a breeding experiment when it was bred at 14 weeks of age with 20-week-old ICR males. Their offspring was analyzed at 3 and 6 weeks of age. (**b**) Macroscopic comparison of 10-week-old outcrossed (C57BL/6J×ICR) EKAREV+ (left) and EKAREV− (middle) females to EKAREV− ICR (right) female. Scale bar: 1 cm. (**c**) The plots show whole-body weights of outcrossed EKAREV+ and EKAREV− 14-week-old females shown as mean ± SD. $N = 13$ EKAREV+, 14 EKAREV−; **** $p \leq 0.0001$ (Student's t-test). (**d**) Estrous cycle stage distribution in the cohort of outcrossed EKAREV+ and EKAREV− females at the time of mammary and ovarian tissue collection at 14 weeks of age. (**e**) Carmine-stained mammary glands of outcrossed 14-week-old EKAREV+ and EKAREV− mice. Scale bar 1 mm. (**f**, **g**) Quantification of mammary epithelial morphological descriptors. The plots show the number of branching points (sum of primary and secondary) (**f**) and the length of epithelial outgrowth (measured from the center of the lymph node to the distal part of the gland) (**g**) as mean ± SD. $N = 13$ EKAREV+, 14 EKAREV−; ns $p \geq 0.05$, * $p \leq 0.05$ (Student's t-test). (**h**) Estrogen receptor (ER), progesterone receptor (PR), and Ki67 expression in the mammary glands of 14-week-old outcrossed EKAREV+ and EKAREV− females. The inserts show details of epithelial areas. Scale bar: 100 µm. (**i**) Quantification of ER+ cells in mammary epithelium. The plot shows mean ± SD. $N = 20$ EKAREV+, 28 EKAREV−; ns $p > 0.05$ (Student's t-test). (**j**) Quantification of PR+ cells in mammary epithelium. The plot shows mean ± SD. $N = 25$ EKAREV+, 32 EKAREV−; * $p \leq 0.05$ (Student's t-test). (**k**) Quantification of Ki67+ cells in mammary epithelium. The plot shows mean ± SD. $N = 9$ EKAREV+, 24 EKAREV−; *** $p \leq 0.001$ (Student's t-test). (**l**, **m**) Level of reproductive hormones (**l**) estrogen and (**m**) progesterone in circulating blood serum. The plots show mean ± SD. $N = 5$ EKAREV+, 7 EKAREV−; ns $p > 0.05$ (Student's t-test). (**n**) Hematoxylin- and eosin-stained sections of ovaries from 14-week-old outcrossed EKAREV+ and EKAREV− mice. Scale bar: 100 µm. (**o**) Quantification of the number of corpora lutea, counted in serial sections of ovaries (taken every 25 µm within the first half of the ovary). The plot shows mean ± SD. $N = 13$ EKAREV+, 14 EKAREV−; * $p \leq 0.05$ (Mann-Whitney test). (**p**) A total number of pups born from the breeding of outcrossed EKAREV+ or EKAREV− females with wild-type ICR male, shown as mean ± SD. $N = 7$ litters from EKAREV+ mothers, 5 litters from EKAREV- mothers; * $p \leq 0.05$ (Student's t-test). (**q**, **r**) Weight of offspring born from the breeding of outcrossed EKAREV+ or EKAREV− females with wild-type ICR male. The plots show the body weight of 3-week-old (**q**) and 6-week-old (**r**) female (pink) and male (blue) pups as mean ± SD. $N = 107$ born pups from 7 EKAREV+ and 5 EKAREV− mothers. ns $p > 0.05$, * $p \leq 0.05$, ** $p \leq 0.01$, *** $p \leq 0.001$, **** $p \leq 0.0001$ (one-way ANOVA for 3 w females and 6 w males, Kruskal-Wallis test for 3 w males and 6 w females)

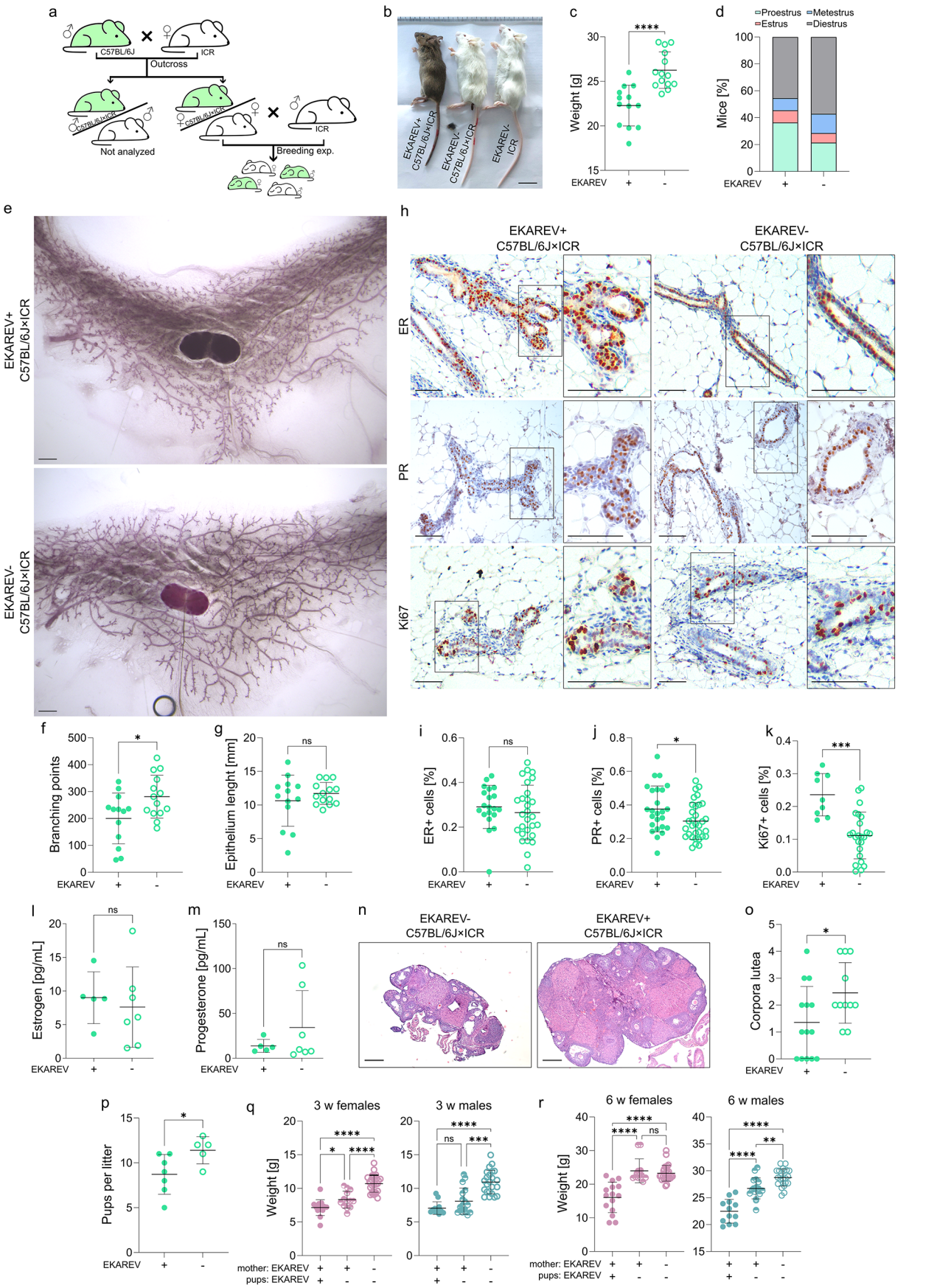
a
C57BL/6J
ICR
Outcross
Not analyzed
Breeding exp.
b
EKAREV+ C57BL/6J×ICR
EKAREV- C57BL/6J×ICR
EKAREV- ICR
c
Weight [g]
EKAREV
d
Proestrus
Metestrus
Estrus
Diestrus
Mice [%]
e
EKAREV+ C57BL/6J×ICR
EKAREV- C57BL/6J×ICR
h
EKAREV+ C57BL/6J×ICR
EKAREV- C57BL/6J×ICR
ER
PR
Ki67
f
Branching points
g
Epithelium lenght [mm]
i
ER+ cells [%]
j
PR+ cells [%]
k
Ki67+ cells [%]
l
Estrogen [pg/mL]
m
Progesterone [pg/mL]
n
EKAREV- C57BL/6J×ICR
EKAREV+ C57BL/6J×ICR
o
Corpora lutea
p
Pups per litter
q
3 w females
3 w males
Weight [g]
mother: EKAREV
pups: EKAREV
r
6 w females
6 w males
Weight [g]
mother: EKAREV
pups: EKAREV

stable biosensor expression in all nuclei in the cells from all experimental animals throughout the imaging period (Fig. 4c). Immunofluorescence staining analysis revealed that the cultured MECs predominantly comprised luminal cells (KRT8+), with less than 1% MECs positively staining for basal cell marker (KRT5+) (Fig. 4c). Thus, further analysis was conducted cumulatively without segregating MEC types.

To analyze ERK activity patterns across different groups, we conducted time-lapse imaging of the EKAREV+MECs for 6 h. For the first hour, the MECs were imaged in a medium without growth factor supplementation to establish baseline ERK activity. Afterwards, fibroblast growth factor 2 (FGF2) was added, and the MECs were imaged for an additional 5 h. The images were processed, segmented, and tracked, and the FRET index was calculated for each individual cell trajectory (Fig. 4b, Supplementary Video 1–4). Individual cell trajectories as well as population averages of ERK activity showed a similar activation pattern in response to FGF2 stimulation across the groups, with most cells reaching maximal activation 20 min after FGF2 addition and returning to baseline activity within 90 min. In contrast, cells from E2-treated mice responded more rapidly, with maximal activity at 10 min, and after the initial peak, they dropped to a slightly higher baseline activity (Fig. 4d, e).

Next, we explored ERK activation patterns in individual cells by single-cell ERK activation wave analysis (Fig. 4b, f-i), assessing basal activity, pulse frequency, wave amplitude, and wave duration before and after FGF2 addition. We found significant differences in basal ERK activity across all groups before (Fig. 4f, top) and after FGF2 addition (Fig. 4f, bottom). ERK activation pulse frequency showed no significant differences between control (C57BL/6J, NT) and hormonally supplemented groups before (Fig. 4g, top) or after (Fig. 4g, bottom) FGF2 addition, but differed significantly between control cells and cells from outcrossed mice. Maximal wave amplitude and duration, key characteristics relevant to cell fate decisions [29, 30], showed slight to no significant differences between groups before FGF2 addition (Fig. 4h, i, top). However, after FGF2 addition, more significant changes in both amplitude and duration were detected in cells from E2P4-treated mice, and in wave duration in cells from outcrossed mice (Fig. 4h, i, bottom), indicating a potential impact on ERK response and possibly changed cellular behavior. Assessment of intervention effects indicated a higher level of intervention-induced variability following the FGF2 addition, especially between C57BL/6J NT and C57BL/6J E2P4, C57BL/6J NT and C57BL/6J×ICR NT, and C57BL/6J E2 or E2P4 and C57BL/6J×ICR NT (Supplementary Fig. 8). Together, these findings demonstrate EKAREV-NLS biosensor functionality but altered MEC responses to external stimuli conveyed via ERK between non-treated, hormone-supplemented and outcrossed mice.

Fig. 4 Primary mammary epithelial cells (MECs) obtained from hormonally supplemented and outcrossed EKAREV+mice exhibit distinct signaling responses. (**a**) Schematic representation of the working principle of the EKAREV-NLS biosensor. The biosensor is located in the nucleus and senses ERK phosphorylation activity. Both reporter fluorescent proteins are detected and FRET to donor ratio is calculated resulting in FRET index values over time. (**b**) Schematic representation of ERK activation wave analysis within individual cells. The FRET index was computed for the baseline and FGF2 response time points. For each wave a fitted sine curve was computed and descriptive wave parameters (basal activity, wave amplitude, wave duration, and pulse frequency) were extracted. (**c**) Representative images of primary MECs with donor (CFP) and FRET (YFP) channels at the first time point, with corresponding endpoint detection of basal (KRT5) and luminal (KRT8) lineage markers. Scale bar: 100 µm. (**d**) Population averages of ERK activity dynamics in response to stimulation with 2.5 nM FGF2, shown as FRET index mean±SD. The gray line at t=0 marks the point of FGF2 addition, the area left of the line represents baseline measurement, and the area right of the line represents the response to FGF2 addition. N=449 for C57BL/6J NT, 391 for C57BL/6J E2, 626 for C57BL/6J E2P4, 484 for C57BL/6J×ICR NT. (**e**) Heatmaps of 50 representative single-cell tracks per experimental variant from panel B. Each row corresponds to a time series of a single cell, the gray line at t=0 marks the point of FGF2 addition. (**f–i**) ERK activation wave analysis, including ERK basal activity (**f**), pulse frequency (**g**), wave maximal amplitude (**h**), and wave maximal duration (**i**) before (up) and after (down) FGF2 addition. The plots show FRET index mean±SD; ns $p>0.05$, *$p\leq0.05$, **$p\leq0.01$, ***$p\leq0.001$, ****$p\leq0.0001$ (Kruskal-Wallis test). NT, non-treated; E2, 17β–estradiol treated; E2P4, 17β–estradiol and progesterone treated; CFP, cyan fluorescent protein; YFP, yellow fluorescent protein; FRET, Förster resonance energy transfer; FGF2, fibroblast growth factor 2; C×I, C57BL/6J×ICR

Discussion

In this study, we investigated the suitability of the EKAREV-NLS biosensor mouse for studying ERK signaling dynamics in the mammary gland and revealed significant reproductive and mammary gland developmental phenotypes associated with biosensor expression. Our findings emphasize the potential systemic effects that can arise from genetically encoded biosensors, even those without previously reported physiological impacts in other tissues, underscoring the complexity of biosensor use in specific biological contexts.

The alterations in mammary gland morphology observed in EKAREV+mice are particularly striking. These mice exhibited significantly impaired epithelial outgrowth and a simplified branching pattern, consistent with the mammary glands of ovariectomized mice and those lacking estrogen or progesterone receptors [31–34]. This phenotype, coupled with smaller body weight, reduced ovarian follicular maturation, disrupted estrous cycles and reduced fertility, suggests a broader dysregulation of female sex hormones. These systemic effects likely stem from the overexpression

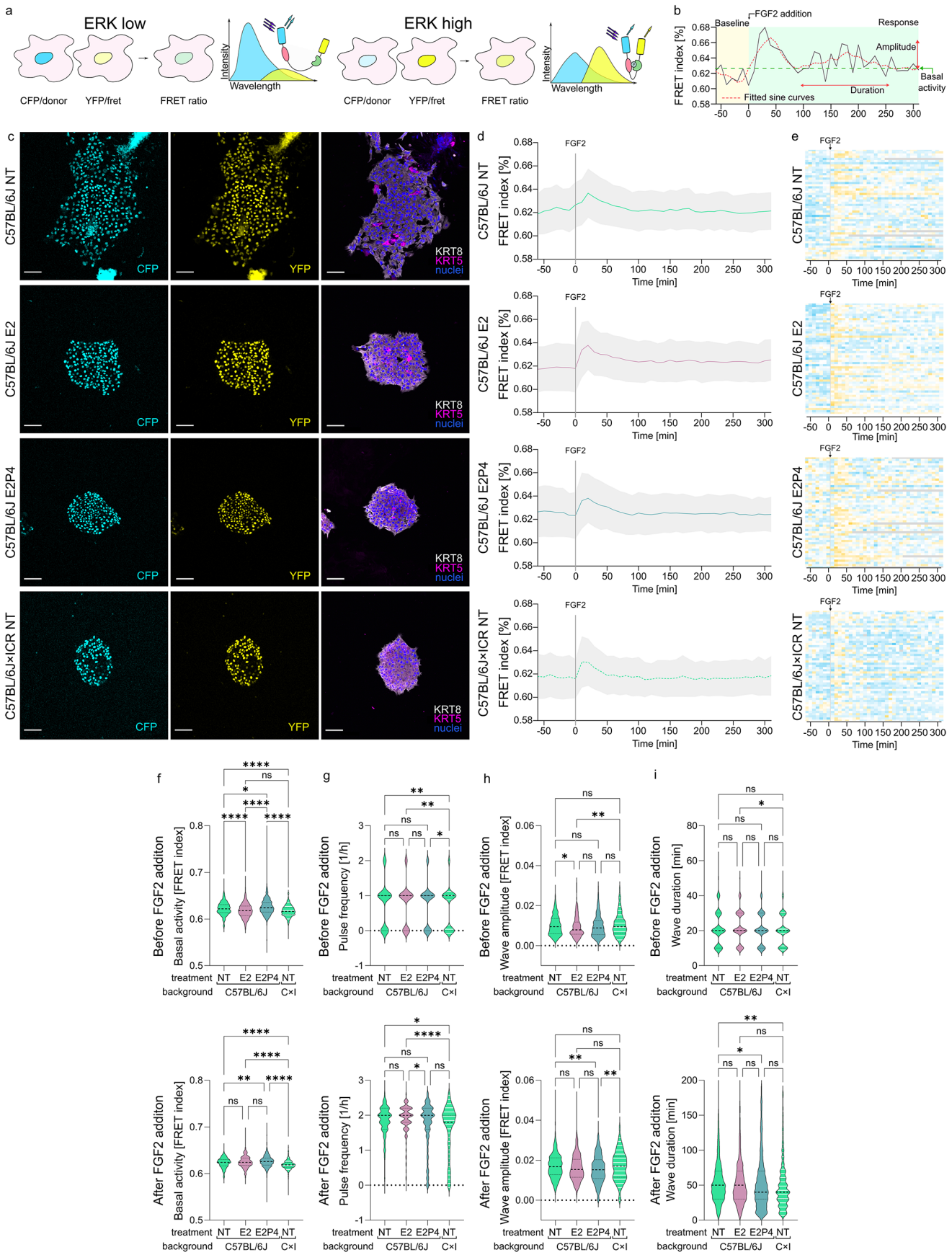
a
ERK low
ERK high
CFP/donor
YFP/fret
FRET ratio
Intensity
Wavelength
b
FGF2 addition
Baseline
Response
Amplitude
Basal activity
Duration
Fitted sine curves
FRET index [%]
c
C57BL/6J NT
C57BL/6J E2
C57BL/6J E2P4
C57BL/6J×ICR NT
CFP
YFP
KRT8
KRT5
nuclei
d
FGF2
FRET index [%]
Time [min]
e
f
Before FGF2 additon
Basal activity [FRET index]
g
Pulse frequency [1/h]
h
Wave amplitude [FRET index]
i
Wave duration [min]
After FGF2 additon
treatment NT E2 E2P4 NT
background C57BL/6J C×I

of the EKAREV biosensor, which supports the notion that biosensor expression levels and genomic integration sites can adversely affect cellular and physiological processes. This aligns with concerns raised by the creators of the strain regarding potential perturbations in endogenous signaling due to high biosensor expression and nuclear localization [12]. The expression level of a transgene is heavily influenced by the number of transgene copies integrated into the genome. Higher transgene copy numbers often lead to increased expression levels, but this relationship is not always straightforward due to potential silencing effects or integration into genomic regions that affect transcription.

The similarity between the phenotypes observed in EKAREV+mice and those of ovariectomized or hormone receptor-deficient mice strongly suggests disrupted hormonal signaling in response to the EKAREV biosensor. Specifically, the glands of post-pubertal nulliparous EKAREV+mice resembled those of prepubertal wild-type mice, indicating impaired responsiveness to estrogen and progesterone, which are crucial for normal mammary ductal elongation and branching [31–34]. Estradiol supplementation partially rescued the mammary epithelial phenotype and reproductive function, improving ductal tree branching and follicular maturation, but was insufficient to fully restore ovulatory cycles and the formation of corpora lutea. This indicates that while estrogen deficiency plays a significant role, other factors, possibly related to hormonal regulation of PR expression, are also impaired. The synergistic action of estradiol and progesterone was necessary for a more robust rescue of mammary branching and growth, underscoring the importance of maintaining proper hormonal signaling for normal mammary development.

Interestingly, outcrossing EKAREV+mice to the ICR strain fully alleviated both the mammary and reproductive phenotypes, suggesting that the observed effects were, at least in part, dependent on the genetic background. The influence of genetic background on mammary gland development and transgenic model phenotypes has been well-documented, with variations in estrogen signaling regulation, mammary tissue responses, and tumor susceptibility recognized across different strains [35, 36]. Different strains and sub-strains vary in epigenetic regulation, promoter activity, and genomic environment, such as structural variations and transposable elements, all of which can influence biosensor expression levels and may contribute to the variation observed in EKAREV+animals [37, 38]. The C57BL/6J strain is known for its stable and predictable transgene expression due to its well-characterized genome, but it may also be more susceptible to deleterious effects associated with high biosensor expression levels or specific transgene integration sites. Outbred strains like ICR are less prone to epigenetic silencing and exhibit greater genomic variability, which may buffer against adverse phenotypes linked to transgene expression [39]. The restoration of normal mammary epithelial development and reproductive function in outcrossed mice suggests the role of strain-specific genetic modifiers in modulating biosensor effects and mitigating the reproductive and developmental challenges. These findings emphasize the importance of considering genetic background when designing and interpreting studies using transgenic biosensor models.

From a biosensor functionality standpoint, we demonstrated that neither hormonal supplementation nor genetic background modification interfered with the EKAREV-NLS biosensor's ability to monitor ERK activity dynamics in mammary epithelial cells. Both interventions maintained stable biosensor expression and enabled effective tracking of ERK activation in response to growth factor stimulation. This suggests that the adjustments we employed to rescue the mammary and reproductive phenotypes do not compromise the utility of the EKAREV-NLS biosensor for studying ERK signaling, making these approaches valuable for future studies in mammary gland biology. Importantly, baseline ERK activity levels remained consistent across all groups, with cells responding uniformly to growth factor stimulation, which confirms the ability to detect dynamic changes in ERK phosphorylation at both the single-cell and population levels.

Most differences between experimental groups were detected in the cellular response following FGF2 stimulation. As estrogen and progesterone can modulate the expression and availability of various signaling constituents associated with ERK [40–42], it is plausible that the prior hormonal exposure influenced cell susceptibility to growth factor stimulation and altered ERK activation dynamics. This highlights the complex interplay between hormonal signaling and ERK activity in mammary tissue, and future studies should aim to elucidate the molecular mechanisms by which these hormones modulate ERK signaling pathways. Furthermore, the differences in response to FGF2 might also be confounded by experimental setup and differences in cell density, cell-to-cell, and cell-to-substrate interactions [43, 44]. Nevertheless, our observations confirm biosensor functionality in all tested conditions and suggest potential changes in cellular ERK responses following these interventions.

In conclusion, while the EKAREV-NLS biosensor is a powerful tool for studying ERK signaling, its expression in mammary epithelial cells leads to significant off-target effects on hormonal signaling and tissue development. Hormonal supplementation and genetic background modification offer viable strategies to mitigate these effects, preserving the utility of the biosensor for studying ERK activity. However, our findings also emphasize the need for

careful consideration of biosensor expression levels, genetic background, and potential systemic effects when employing genetically encoded biosensors in vivo. Future research should aim to further elucidate the molecular mechanisms underlying these biosensor-induced phenotypes and explore the potential for optimizing biosensor expression to minimize adverse effects on tissue development and function.

Limitations of the Study

This study faced several limitations, primarily due to the challenges of maintaining sufficient numbers of female EKAREV+C57BL/6J mice. Since the reanimation of the transgenic strain, the breeding performance of this line was suboptimal, and the litter sizes progressively declined over time. Consequently, the number of EKAREV+C57BL/6J females available for experimentation was significantly reduced, which limited the statistical power of some experiments and observations. These constraints restricted our ability to comprehensively evaluate certain aspects of mammary epithelial outgrowth and hormone supplementation effects across broader experimental cohorts. Further, the reduced availability of the EKAREV+C57BL/6J females, together with the low amount of mammary epithelium from them, limited our capability of conducting experiments to assess the biological effects of altered ERK wave characteristics in cells from hormone-supplemented and non-treated animals. This constraint prevented a comprehensive evaluation of the downstream physiological consequences associated with the observed signaling changes.

Materials and Methods

Experimentation with Animals

All experiments involving mice were performed under the approval of the Ministry of Education, Youth and Sports of the Czech Republic (license # MSMT-24093/2021-3), supervised by the Expert Committee for Laboratory Animal Welfare of the Faculty of Medicine, Masaryk University, at the Laboratory Animal Breeding and Experimental Facility of the Faculty of Medicine, Masaryk University (LABEF FM MU; facility license 310 #58013/2017-MZE-17214). All animals were housed in individually ventilated or open cages, with an ambient temperature of 22 °C, 40–60% humidity, a 12 h:12 h light: dark cycle, and food and water *ad libitum*. The EKAREV-NLS mice (Eisuke-NLS; B6-Tg(EKAREV)pT2A-3905NLS) were reconstituted from frozen sperm obtained from the Laboratory Animal Resource Bank at NIBIOHN, Japan on C57BL/6J at the Czech Centre for Phenogenomics and maintained on the C57BL/6J background unless outcrossed. To generate experimental animals on C57BL/6J background, EKAREV− females were bred with EKAREV+males, as recommended by the strain supplier. For outcrossing experiments, EKAREV+C57BL/6J males were crossed with wild-type ICR females (obtained from the LABEF FM MU). The mice were genotyped by detection of green fluorescence of the transgene in ear punches using a fluorescence microscope.

For hormone supplementation experiments, pubertal (8-9-week-old) EKAREV+and EKAREV− C57BL/6J females from the same litter were divided into three experimental groups; nontreated control (NT), estradiol-treated (E2), and estradiol-progesterone-treated (E2P4). EKAREV− C57BL/6J females from the same litter were used as developmental control and housed in the same cage as the NT group. Hormones were supplied in drinking water, 500 ng/ml estradiol (E2 group) or 500 ng/ml progesterone with 50 ng/ml estradiol (E2P4 group), over five weeks, with water changed twice per week, on Mondays and Fridays. The E2 group was constantly provided with fresh estradiol-supplemented water on both Mondays and Fridays. The E2P4 group was provided with fresh estradiol-supplemented water on Mondays and with fresh progesterone-supplemented water on Fridays. The cages housed 3 to 5 animals per treatment and water consumption was not recorded.

To assess female breeding performance, 14-week-old EKAREV+C57BL/6J or EKAREV+C57BL/6J×ICR females were mated with 20-week-old wild-type ICR males for one week, then the males were moved to separation. Females were monitored to assess pregnancy, giving birth, litter size and survival, and maternal behavior. The offspring were assessed for genotypes, general appearance, and weight (measured at 3 and 6 weeks of age).

Hormone Level Analysis

Blood was collected by cardiac punction from mice anesthetized by isoflurane inhalation. Blood was left for 20 min at RT to allow for the clotting, subsequently centrifuged at 2000 × g for 10 min and the supernatant was collected. Circulating hormone levels were assessed by commercially available ELISA kits Estradiol Parameter Assay Kit (#KGE014, R&D Systems) and Mouse Progesterone ELISA Kit (#NBP2-60125, Novus Biological). All procedures were performed according to the manufacturer's protocols with minor modifications. Briefly, samples were centrifuged for 10 min at 4 °C and 2000 × g to remove any precipitation. The serum for the estradiol detection underwent pretreatment according to the manufacturer's instructions with volumes adjusted to the available sample volume, then the

samples were used in the volume of 50 µl. No changes to the protocol were made for progesterone detection.

Histological and Immunohistochemical Staining

The right thoracal (#3) mammary gland and the right ovary were collected for paraffin embedding. The tissues were fixed overnight in 4% paraformaldehyde (PFA), dehydrated, and paraffin-embedded. The paraffin-embedded tissues were cut into 5 µm sections and stained with hematoxylin and eosin (HE) or immunostained. For immunohistochemical staining, the slides were deparaffinized, incubated in target retrieval solution, pH 9 (#S2367, Dako) for 30 min at 98 °C and blocked with 3% hydrogen peroxide, for 10 min at RT, and 10% FBS in PBS for 30 min at RT. After blocking, the slides were incubated with the primary antibodies (Estrogen Receptor α (D-12) Mouse mAb, #sc-8005, Santa Cruz Biotechnology, 1:200; Progesterone Receptor A/B (D8Q2J) XR® Rabbit mAb, #8757S, Cell Signaling; 1:200 and Ki-67 Rabbit mAb, #RBK027, ZYTOMED Systems, 1:200) in 10% FBS in PBS at 4 °C overnight. After washing, the slides were incubated with EnVision+ System-HRP Labelled Polymer Anti-Rabbit (#K4003, Dako) or Anti-Mouse (#P0447, Dako), counterstained with hematoxylin and mounted in Pertex.

For the whole mount carmine staining, the right inguinal (#4) gland was collected, fixed overnight in Carnoy's fixative (100% ethanol: chloroform: glacial acetic acid at 6:3:1 ratio), washed in 70% ethanol, gradually rehydrated to distilled water and stained in Carmine Alum solution (1% carmine, 0.5% aluminum potassium sulfate) at 4 °C overnight. Then the tissues were dehydrated in increasing ethanol series and cleared by incubation in BioClear (Bio-Optica) for several days, and imaged on M165 FC microscope (Leica) controlled by Leica Application Suite X software.

Endpoint vaginal smears were collected at the time of the sacrifice on glass slides, left at RT to dry, immersed in 70% ethanol, and stored at 4 °C before staining them according to the standard protocol for Papanicolaou (PAP) staining. PAP-stained samples and H&E-stained sections were imaged using a DM5000 microscope (Leica) controlled by Leica Application Suite X software.

Primary mammary epithelial cultures were fixed with 4% PFA for 15 min at RT and subsequently washed 3 times with 1× PBS. After permeabilization with 0.05% Triton X-100 in PBS for 10 min at RT, the samples were blocked with 10% FBS in PBS for 30 min at RT and then incubated with primary antibodies (Rabbit Polyclonal Anti Keratin 5, #905504, and Mouse Polyclonal Anti Keratin 8, #904804, both from BioLegend; both at 1:250) at 4 °C overnight, and secondary antibodies (anti-rabbit Alexa Fluor™ 568, #A11036, and anti-mouse Alexa Fluor™ 633, #A21052, both from Invitrogen; both at 1:500 dilution) for 30 min at RT. The stained cells were imaged on an inverted microscope Zeiss Axio Observer.7 with laser scanning unit LSM 880, Axiocam MRm, and Plan Apo 25× multi-immersion objective (NA = 0.80) (all ZEISS) with glycerol immersion.

Primary Mammary Epithelium Isolation, Culture and Imaging

Mammary epithelial fragments (primary organoids) were isolated according to the previously established protocol [45]. In short, mammary glands (left thoracal and inguinal glands, #3, 4, and 5) were collected, minced, and digested in a digestion solution [2 mg/ml collagenase (Merck), 2 mg/ml trypsin (Thermo Fisher Scientific), 5 µg/ml insulin, 50 µg/ml gentamicin (both Merck), 5% fetal bovine serum (Biosera) in DMEM/F12 (Thermo Fisher Scientific)] for 30 min at 37 °C. Following treatment with DNase I (20 U/ml; Merck), organoids were separated from the stromal fraction by differential centrifugation. The organoids were seeded in basal organoid medium (BOM; 1× ITS (10 µg/ml insulin, 5.5 µg/ml transferrin, 6.7 ng/ml sodium selenite), 100 U/ml of penicillin and 100 µg/ml of streptomycin in DMEM/F12) on 2% Matrigel-coated 8-well slide chambers (ibidi) at the density of 50 organoids/well and allowed to completely attach to the bottom (about 3 days) before they were used for the time-lapse imaging experiments.

Time-lapse imaging was performed in phenol red-free BOM for a total duration of 6 h; first, the baseline acquisition was performed for 1 h in BOM without growth factor supplementation, then FGF2 (Enantis) was added to the final concentration of 2.5 nM and the imaging was continued for additional 5 h. The images were acquired every 10 min using an inverted Zeiss Axio Observer.7 (ZEISS) microscope equipped with laser scanning unit LSM 880 (ZEISS) and Plan Apo 25× multi-immersion objective (NA = 0.80; ZEISS) with water immersion. The biosensor CFP-YFP was excited with a 405 nm laser, and the PMT detectors with wavelengths set to 461–503 nm (CFP) and 508–597 nm (YFP) were used for emission detection. Images were acquired using laser-based autofocus with an Axiocam MRm (ZEISS) camera at 16-bit depth. The microscope was controlled by Zen Black software (ZEISS). The environmental conditions (37 °C, 5% CO_2) were controlled through a custom-made incubator controller (EMBL, Christian Kaiser). Cells were subsequently fixed with 4% PFA for immunostaining.

Image Processing, Analysis and Data Extraction

The sample processing, image acquisition, data extraction and analysis were done by one researcher and were

not performed in a blinded fashion. Wholemount carmine images were analyzed in Fiji [46] by manually counting primary and secondary branching points and measuring epithelium area and length from the center of the lymph node to the most distal epithelial end. Vaginal smear images were visually inspected by two independent researchers to assign estrous cycle phases. Numbers of PR+cells in mammary gland sections were quantified using QuPath software [47]. Follicle types were manually counted from serial ovarian sections (each follicle counted only once if spanning multiple sections).

Timelapse images were processed in ZEN Blue (ZEISS), Imaris (Oxford Instruments), and Image J [46] software. Shortly, the background was subtracted from both channels, and a Gaussian filter was applied to smooth out the signal. Image segmentation, object recognition, tracking, and video generation were performed in Imaris. Segmented mask images were further processed in ImageJ to generate FRET index visualizations by dividing the raw FRET image by the raw donor image. Numerical data extracted from raw FRET and donor channel images was exported and further analyzed in Excel and GraphPad Prism.

FRET Wave Analysis

Numerical data extracted from tracked images was processed in Excel. The FRET index was calculated according to the following formula $FRETindex\ [\%] = \frac{FRETi}{DONORi+FRETi}$ and subsequently used for wave analysis. Single-cell wave analysis was performed by denoising individual cell measurements by applying a point rolling average. Subsequently, the basal activity of each wave was determined together with local maxima, following what maximal amplitude, duration, and oscillation frequency were calculated. Population averages and heat maps were created from raw FRET index data. The resulting values were plotted and statistically processed in GraphPad Prism.

Statistical Analysis

Sample size was not determined a priori and experiments together with analysis were not done in a blinded fashion. Statistical analysis was performed in GraphPad Prism version 10 (Dotmatics). The Student's t-test (unpaired, two-tailed) or Mann-Whitney test were used for the comparison of two groups depending on the data normality distribution determined by the Shapiro-Wilk normality test. For the comparison of 3 or more groups, one-way ANOVA or nonparametric Kruskal–Wallis test was used depending on the data normality distribution. All plots were generated in GraphPad Prism and show mean ± SD; ns $P > 0.05$, $*P < 0.05$, $**P < 0.01$, $***P < 0.001$, $****P < 0.0001$. The number of independent biological replicates is indicated as n, while N indicates the total number of analyzed units (e.g. animals, samples, or cells).

Supplementary Information The online version contains supplementary material available at https://doi.org/10.1007/s10911-025-09574-8.

Acknowledgements We thank Denisa Belisova for her help with mouse husbandry and hormonal treatments and Vaclav Chochola for the EnVision+ System-HRP Labelled Polymer. We acknowledge the CEITEC core facility CELLIM supported by MEYS CR (LM2023050 Czech-BioImaging) for their support in obtaining data presented in this paper.

Author Contributions M.B. performed all experiments, analyzed data, prepared figures, and wrote the manuscript. Z.S.K. conceptualized the study, acquired funding for the study, and wrote the manuscript.

Funding This work was funded by grants from Masaryk University (MUNI/G/1775/2020, MUNI/A/1301/2022), Czech Science Foundation (GAČR; GA23-04974S), and the Ministry of Education, Youth and Sports of the Czech Republic (MEYS CR; ERC CZ LL2323 FIBROFORCE). M.B. is a holder of the Brno PhD Talent Scholarship, funded by the Brno City Municipality.

Data Availability No datasets were generated or analysed during the current study.

Declarations

Competing Interests Z.S.K. is the Editor-in-Chief of the Journal of Mammary Gland Biology and Neoplasia. M.B. has no competing interest.

References

1. Tao W, Evans B-G, Yao J, Cooper S, Cornetta K, Ballas CB, et al. Enhanced green fluorescent protein is a nearly ideal long-term expression tracer for hematopoietic stem cells, whereas DsRed-express fluorescent protein is not. Stem Cells. 2007;25:670–8.
2. Klein RL, Dayton RD, Leidenheimer NJ, Jansen K, Golde TE, Zweig RM. Efficient neuronal gene transfer with AAV8 leads to

neurotoxic levels of tau or green fluorescent proteins. Mol Ther. 2006;13:517–27.
3. Taghizadeh RR, Sherley JL. CFP and YFP, but not GFP, provide stable fluorescent marking of rat hepatic adult stem cells. J Biomed Biotechnol. 2008;2008:453590.
4. Liu HS, Jan MS, Chou CK, Chen PH, Ke NJ. Is green fluorescent protein toxic to the living cells? Biochem Biophys Res Commun. 1999;260:712–7.
5. Ganini D, Leinisch F, Kumar A, Jiang J, Tokar EJ, Malone CC, et al. Fluorescent proteins such as eGFP lead to catalytic oxidative stress in cells. Redox Biol. 2017;12:462–8.
6. Goto H, Yang B, Petersen D, Pepper KA, Alfaro PA, Kohn DB, et al. Transduction of green fluorescent protein increased oxidative stress and enhanced sensitivity to cytotoxic drugs in neuroblastoma cell lines. Mol Cancer Ther. 2003;2:911–7.
7. Coumans JVF, Gau D, Poljak A, Wasinger V, Roy P, Moens P. Green fluorescent protein expression triggers proteome changes in breast cancer cells. Exp Cell Res. 2014;320:33–45.
8. Comley LH, Wishart TM, Baxter B, Murray LM, Nimmo A, Thomson D, et al. Induction of cell stress in neurons from transgenic mice expressing yellow fluorescent protein: implications for neurodegeneration research. PLoS ONE. 2011;6:e17639.
9. Ansari AM, Ahmed AK, Matsangos AE, Lay F, Born LJ, Marti G, et al. Cellular GFP toxicity and immunogenicity: potential confounders in in vivo cell tracking experiments. Stem Cell Rev Rep. 2016;12:553–9.
10. Huang WY, Aramburu J, Douglas PS, Izumo S. Transgenic expression of green fluorescence protein can cause dilated cardiomyopathy. Nat Med. 2000;6:482–3.
11. Gasterstädt I, Jack A, Stahlhut T, Rennau L-M, Gonda S, Wahle P. Genetically encoded calcium indicators can impair Dendrite growth of cortical neurons. Front Cell Neurosci. 2020;14:570596.
12. Kamioka Y, Sumiyama K, Mizuno R, Sakai Y, Hirata E, Kiyokawa E, et al. Live imaging of protein kinase activities in transgenic mice expressing FRET biosensors. Cell Struct Funct. 2012;37:65–73.
13. Harvey CD, Ehrhardt AG, Cellurale C, Zhong H, Yasuda R, Davis RJ, et al. A genetically encoded fluorescent sensor of ERK activity. Proc Natl Acad Sci U S A. 2008;105:19264–9.
14. Komatsu N, Aoki K, Yamada M, Yukinaga H, Fujita Y, Kamioka Y, et al. Development of an optimized backbone of FRET biosensors for kinases and GTPases. Mol Biol Cell. 2011;22:4647–56.
15. Mizuno R, Kamioka Y, Kabashima K, Imajo M, Sumiyama K, Nakasho E, et al. In vivo imaging reveals PKA regulation of ERK activity during neutrophil recruitment to inflamed intestines. J Exp Med. 2014;211:1123–36.
16. Muta Y, Fujita Y, Sumiyama K, Sakurai A, Taketo MM, Chiba T et al. Composite regulation of ERK activity dynamics underlying tumour-specific traits in the intestine. Nat Commun. 2018;9.
17. Hiratsuka T, Fujita Y, Naoki H, Aoki K, Kamioka Y, Matsuda M. Intercellular propagation of extracellular signal-regulated kinase activation revealed by in vivo imaging of mouse skin. Elife. 2015;4:e05178.
18. Aoki K, Kondo Y, Naoki H, Hiratsuka T, Itoh RE, Matsuda M. Propagating Wave of ERK Activation orients collective cell Migration. Dev Cell. 2017;43:305–e3175.
19. Kumagai Y, Naoki H, Nakasyo E, Kamioka Y, Kiyokawa E, Matsuda M. Heterogeneity in ERK activity as visualized by in vivo FRET imaging of mammary tumor cells developed in MMTV-Neu mice. Oncogene 2015. 2014;34:8.
20. Richardson FL. The relative growth of the mammary glands in normal, ovariectomized and adrenalectomized female mice. Anat Rec. 1955;123:279–89.
21. Haslam SZ. The ontogeny of mouse mammary gland responsiveness to ovarian steroid hormones. Endocrinology. 1989;125:2766–72.
22. Crabtree JS, Zhang X, Peano BJ, Zhang Z, Winneker RC, Harris HA. Development of a mouse model of mammary gland versus uterus tissue selectivity using estrogen- and progesterone-regulated gene markers. J Steroid Biochem Mol Biol. 2006;101:11–21.
23. Gordon MN, Osterburg HH, May PC, Finch CE. Effective oral administration of 17 beta-estradiol to female C57BL/6J mice through the drinking water. Biol Reprod. 1986;35:1088–95.
24. Haslam SZ, Shyamala G. Effect of oestradiol on progesterone receptors in normal mammary glands and its relationship with lactation. Biochem J. 1979;182:127–31.
25. Barnett KR, Schilling C, Greenfeld CR, Tomic D, Flaws JA. Ovarian follicle development and transgenic mouse models. Hum Reprod Update. 2006;12:537–55.
26. MacLennan MB, Anderson BM, Ma DWL. Differential mammary gland development in FVB and C57Bl/6 mice: implications for breast cancer research. Nutrients. 2011;3:929–36.
27. Aupperlee MD, Drolet AA, Durairaj S, Wang W, Schwartz RC, Haslam SZ. Strain-specific differences in the mechanisms of progesterone regulation of murine mammary gland development. Endocrinology. 2009;150:1485–94.
28. Chia R, Achilli F, Festing MFW, Fisher EMC. The origins and uses of mouse outbred stocks. Nat Genet. 2005;37:1181–6.
29. Kocieniewski P, Lipniacki T. MEK1 and MEK2 differentially control the duration and amplitude of the ERK cascade response. Phys Biol. 2013;10:035006.
30. Ryu H, Chung M, Dobrzyński M, Fey D, Blum Y, Lee SS, et al. Frequency modulation of ERK activation dynamics rewires cell fate. Mol Syst Biol. 2015;11:838.
31. Curtis Hewitt S, Couse JF, Korach KS. Estrogen receptor transcription and transactivation: estrogen receptor knockout mice: what their phenotypes reveal about mechanisms of estrogen action. Breast Cancer Res. 2000;2:345–52.
32. Conneely OM, Mulac-Jericevic B, Lydon JP, De Mayo FJ. Reproductive functions of the progesterone receptor isoforms: lessons from knock-out mice. Mol Cell Endocrinol. 2001;179:97–103.
33. Mulac-Jericevic B, Lydon JP, DeMayo FJ, Conneely OM. Defective mammary gland morphogenesis in mice lacking the progesterone receptor B isoform. Proc Natl Acad Sci U S A. 2003;100:9744–9.
34. Lydon JP, DeMayo FJ, Funk CR, Mani SK, Hughes AR, Montgomery CA, et al. Mice lacking progesterone receptor exhibit pleiotropic reproductive abnormalities. Genes Dev. 1995;9:2266–78.
35. Jerry DJ, Shull JD, Hadsell DL, Rijnkels M, Dunphy KA, Schneider SS, et al. Genetic variation in sensitivity to estrogens and breast cancer risk. Mamm Genome. 2018;29:24–37.
36. Wadia PR, Vandenberg LN, Schaeberle CM, Rubin BS, Sonnenschein C, Soto AM. Perinatal bisphenol A exposure increases estrogen sensitivity of the mammary gland in diverse mouse strains. Environ Health Perspect. 2007;115:592–8.
37. Ferraj A, Audano PA, Balachandran P, Czechanski A, Flores JI, Radecki AA, et al. Resolution of structural variation in diverse mouse genomes reveals chromatin remodeling due to transposable elements. Cell Genomics. 2023;3:100291.
38. Lilue J, Doran AG, Fiddes IT, Abrudan M, Armstrong J, Bennett R et al. Sixteen diverse laboratory mouse reference genomes define strain-specific haplotypes and novel functional loci. Nat Genet. 2018;50(11):1574–83.
39. CD-1®. IGS Mouse | Charles River.
40. Lavoie H, Gagnon J, Therrien M. ERK signalling: a master regulator of cell behaviour, life and fate. Nat Rev Mol Cell Biol. 2020;21(10):607–32.
41. Sternlicht MD, Sunnarborg SW, Kouros-Mehr H, Yu Y, Lee DC, Werb Z. Mammary ductal morphogenesis requires paracrine activation of stromal EGFR via ADAM17-dependent shedding of epithelial amphiregulin. Development. 2005;132:3923–33.

42. Mallepell S, Krust A, Chambon P, Brisken C. Paracrine signaling through the epithelial estrogen receptor alpha is required for proliferation and morphogenesis in the mammary gland. Proc Natl Acad Sci U S A. 2006;103:2196–201.
43. Aoki K, Kumagai Y, Sakurai A, Komatsu N, Fujita Y, Shionyu C, et al. Stochastic ERK activation induced by noise and cell-to-cell propagation regulates cell density-dependent proliferation. Mol Cell. 2013;52:529–40.
44. Crozet F, Levayer R. Emerging roles and mechanisms of ERK pathway mechanosensing. Cell Mol Life Sci. 2023;80:355.
45. Koledova Z, Lu P. A 3D fibroblast-epithelium co-culture model for understanding Microenvironmental Role in branching morphogenesis of the mammary gland. Methods Mol Biol. 2017;1501:217–31.
46. Schindelin J, Arganda-Carreras I, Frise E, Kaynig V, Longair M, Pietzsch T, et al. Fiji: an open-source platform for biological-image analysis. Nat Methods. 2012;9:676–82.
47. Bankhead P, Loughrey MB, Fernández JA, Dombrowski Y, McArt DG, Dunne PD, et al. QuPath: open source software for digital pathology image analysis. Sci Rep. 2017;7:16878.